## PAPER

Check for updates

# CO oxidization catalyzed by B, N, and their co-doped fullerenes: a first-principles investigation†

Boya Gao and Gang Chen ⓘD *

Using the elastic band method based on first-principles calculations, we have carefully studied the catalytic properties of B, N, and their co-doped fullerenes. During oxidization of CO, both $C_{59}B$ and $C_{59}N$ can be oxidized to form durable oxide catalysts for successive CO oxidizations, the rate determining steps of which have 0.59 and 0.80 eV barriers, respectively. In CO-rich conditions, the $C_{59}N$ may remain in the entire reaction cycle with a 0.44 eV rate determining barrier. Both BN-pair doped fullerene and B-rich $B_3N$ doped fullerene can also be oxidized during the process of catalyzing CO oxidizations, and the oxides can then be repeatedly used as catalysts in successive CO oxidizations with rate determining barriers of approximately 0.42 eV. The central B in the N-rich $C_{56}BN_3$ is protected by its surrounding N atoms against oxidization to remain as a durable catalyst, the rate determining barrier of which is 0.63 eV for catalyzing CO oxidization. These results for the B and N doped fullerenes, and especially for the B–N co-doped fullerenes, could help in the design of high-performance non-metal catalysts, calling for further detailed experimental investigations.

## 1.  Introduction

The increased energy demand and the corresponding rapid consumption of various fuels have attracted extraordinary research interests that are focused on environmental pollutants. Among these CO has been identified as a poisonous pollutant species and has already aroused intensive research attention during the past few decades. It is usually generated by incomplete combustion of various fossil energy sources, for example emissions from vehicle exhaust fumes, various industrial processes, the consumption of fossil energy materials, and so forth. It can bind to hemoglobin more strongly than $O_2$ to reduce oxygen availability for different organs, resulting in impaired concentration, slow reflexes, and confusion. In addition, CO in fuel cells is a critical and harmful issue, especially with regard to the large-scale application of fuel cells as sustainable energy carriers, which could poison the electrode making it inactive. With regard to cleaning, effective heterogeneous catalysts for CO oxidation play a critical role. Usually, precious metals or their related alloys or oxides are needed for catalysis of the CO oxidation reaction, for example Pt, Au, Ru, Rh, and Pd.[1–23] However, these metal catalysts are expensive and usually need to be used at a high temperature to achieve an efficient operation. Finding inexpensive alternatives to replace these precious metal-based catalysts is therefore highly desirable. Therefore, investigation of low-priced metal-free catalysts has gained tremendous research interest in recent decades.

Recently, carbon or carbon-based nanomaterials have been found to have superior catalytic properties, and a significant amount of research has been focused on exploring non-metal catalysts. These carbon nanomaterials, which have $sp^2$-like hybridization networks including graphene, nanotubes, fullerene, and so forth, have abundant free-flowing π electrons to provide reactions requiring electrons, and this makes them potential base materials for exploring high-performance metal-free catalysts. However, the π electrons in ideal $sp^2$-like nanostructures, such as $C_{60}$, are too inert to be directly used to catalyze reactions. In recent years, studies have shown that breaking the integrity of the π electron distribution in heteroatom doped $sp^2$-like nanostructures could activate π electrons, giving them superior catalytic properties.[24–27] Owing to the difference in the number of valence electrons, B and N are the most frequently studied heteroatom doping species. The doped $C_{60}$ structures with a maximum number of doped B and N were previously studied by Manaa *et al.*[28–30] N doping can cause conjugation of the lone-pair electrons with the carbon π electrons to allow the surrounding C atoms to become active for $O_2$ adsorption. In contrast, the doping of the electron deficient B atom in carbon networks can only provide a vacant $2p_z$ orbital for conjugation with carbon π electrons, resulting in B becoming an active site for $O_2$ adsorption. Hu *et al.*[31] and Lin *et al.*[32] studied the CO oxidations catalyzed by N doped carbon nanotubes using density functional theory (DFT) calculations. Chen and his co-workers reported DFT studies on CO

*School of Physics and Technology, University of Jinan, Shandong 250022, China. E-mail: ss_cheng@ujn.edu.cn*

oxidizations catalyzed by N doped $C_{60}$ (ref. 33) and penta-graphene.[34] In addition, B, N, P, and Si-doped graphene also shows superior reactivities for catalyzing CO oxidizations.[35–39] Despite the great progress that has been made in the search for heteroatom doped carbon nanostructure catalysts, studies providing detailed reaction paths are still highly desired to give deeper insights into the catalytic origin, aiming to help researchers design high-performance and durable metal free catalysts. To the best of our knowledge, comparative theoretical studies on the catalytic properties of B, N and their co-doped $C_{60}$ are limited and there are no detailed studies on the catalytic properties of the corresponding oxides of doped $C_{60}$, which are the by-products of the pioneering CO oxidizations.

In this paper, by using B or N doped $C_{60}$, and their co-doped fullerenes as prototype nanostructure catalysts, we carefully studied the minimum energy reaction paths of CO oxidizations by using the elastic band method based on first-principles calculations. Our studies suggest that the carbon-based nanostructures would experience oxidization during catalyzing CO oxidizations. The catalytic properties of these oxides are investigated for the first time, as these could then act as durable recycling high-performance catalyst species for successive CO oxidization cycles. Furthermore, our studies on the BN-pair, $BN_3$, and $B_3N$ doped $C_{60}$ could shed light on the development of metal-free catalysts by using small B–N co-doping motifs, either in stoichiometric or B- and N-rich conditions.

## 2.   Computational details

We have carried out detailed minimum energy reaction path studies based on first-principles calculations which were performed within the framework of spin-polarized DFT as implemented in the Vienna *ab initio* simulation package (VASP).[40] The projector augmented-wave method was employed and a cutoff energy of 400 eV was used for the plane wave bases to construct the wave functions.[41] The exchange–correlation energy was calculated by using generalized gradient approximation (GGA) with the Perdew, Burke, and Ernzerhof (PBE) parameterized functional.[42] In order to mimic the zero-dimensional materials, a supercell with a vacuum space of more than 10 Å was employed to clearly separate the cluster and its periodic images in order to eliminate the interaction between them. For such a large supercell, only the $\Gamma$ point was used to integrate the electronic properties in the first Brillouin zone. The convergence criterion of the electronic properties was set to $10^{-5}$ eV. The positions of the atoms were fully optimized until the maximum force acting on each atom converged to 0.01 eV $Å^{-1}$. For the minimum energy path, we first carried out a 16-image nudged elastic band method (NEB) calculation. Based on the optimized NEB path, we re-optimized the reaction path by using the elastic band method with a dense image set around the saddle point along the reaction path, with the purpose of obtaining a sense of the accurate energy barrier.[43–45] Along the entire reaction cycle, we compared the calculated barriers and chose the largest one as the rate determining barrier. The adsorption energy was calculated by referring to the free-standing gas molecule and nanostructure:

$$E_{ads} = E_{fullerene+molecule} - E_{fullerene} - E_{molecule}$$

In which $E_{fullerene+molecule}$, $E_{fullerene}$, and $E_{molecule}$ were the total energies of the molecule adsorbed structure, the doped fullerene, and the isolated molecule, respectively. A negative value indicates an exothermic process. In addition, we also calculated the frequencies of the initial, transition, and final states of all of the studied reaction paths. The vibration properties were studied by using the linear response method as implemented in the VASP code.

## 3.   Results and discussion

### 3.1   Catalytic properties of B and N doped fullerenes

**3.1.1   Gas molecule adsorption on $C_{59}B$ and $C_{59}N$.** We started our studies by considering the adsorptions of $O_2$ and CO small gas molecules on the singly doped fullerenes. Firstly, we calculated the formation energy of the doped structure using:

$$E_f = \frac{E_{C_{60-n}X_n} - (60-n)\mu_C - n\mu_X}{60}$$

In which $E_{C_{60-n}X_n}$ is the total energy of the doped configuration. X represents B or N. $\mu_C$ and $\mu_X$ are the chemical potentials of C in graphene and X in its bulk. Although $C_{60}$, $C_{59}B$, and $C_{59}N$ were calculated to have formation energies of 0.373, 0.387, and 0.380 eV, they have previously been fabricated in experiments. In order to estimate their stabilities, we performed first-principles molecular dynamics simulations (FPMD) at 1000 K, which last for 5 ps with a time step of 1 fs. The geometrical structures are found to be retained during our FPMD studies, suggesting their stability. Once they were formed in the experiments, they could be then used as catalysts for CO oxidization. Both CO and $O_2$ could be exothermically adsorbed onto $C_{59}B$, the lowest energy adsorption configurations for which are shown in Fig. 1a and b, respectively. The corresponding adsorption energies are −0.80 and −1.02 eV. Our elastic band method studies show that CO adsorption is barrierless. The reaction energy, such as the energy barrier, is defined as:

$$E_{reaction} = E_{inter} - E_{initial}$$

In which the $E_{inter}$ and $E_{initial}$ are the calculated total energies of the intermediate state along the reaction path and the initial reaction state, respectively. A positive value indicates there is an energy cost to activate the reaction. However, the $O_2$ must first overcome the 0.06 eV energy barrier to cap onto the B atom in an end-on adsorption configuration (see Fig. 1c), then reach the final chemisorption state by overcoming a 0.05 eV energy barrier. In the final adsorption state, the O atoms connect with the B and its adjunct C atoms. The O–O bond is roughly parallel to the B–C bond below. The bonding between O and $C_{59}B$ results in a charge transfer of approximately 0.86$e$ (calculated using the Bader analysis technique[46]) from $C_{59}B$ to $O_2$ to elongate the O–O bond by 0.19 Å to activate the $O_2$, which is close to previously reported results.[33,47–49] In our calculation, the $O_2$ is
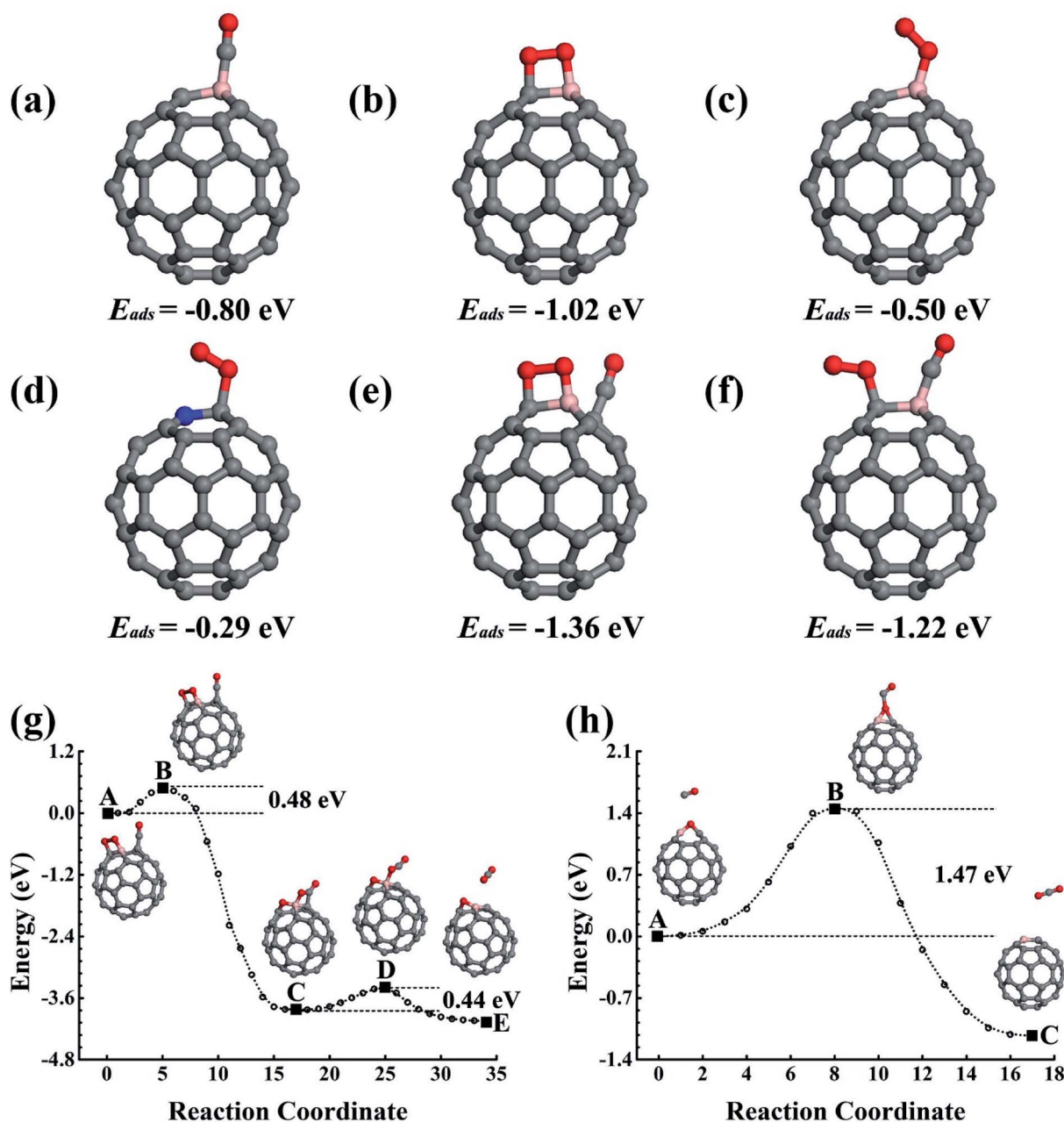
Fig. 1 The structures of CO adsorption (a), $O_2$ adsorption (b) and (c), and CO and $O_2$ co-adsorption (e) and (f) on $C_{59}B$. (d) The lowest energy structure of $O_2$ molecules on $C_{59}N$. The adsorption energies are also given. (g) and (h) Show the reaction paths for CO oxidization catalyzed by $C_{59}B$. The initial, final, saddle, and meta-stable intermediate states are illustrated in the inset figures. C, B, N, and O are represented by the grey, pink, blue, and red balls.

found in the $^3\Sigma_g^-$ triplet ground state before adsorption onto $C_{59}B$. When it gets close enough to $C_{59}B$ to adsorb onto it, a charge transfer would occur. In the final adsorption state, the charge gain elongates the O–O bond and transfers it into the $^1\Delta_g$ singlet excited state. In contrast to the gas adsorption on $C_{59}B$, the $C_{59}N$ can only adsorb $O_2$, for which our elastic band method calculations did not find a barrier. The adsorption energy was calculated to be −0.29 eV. The $O_2$ could only be adsorbed in an end-on adsorption configuration as shown in Fig. 1d with one of its O atoms being connected to the adjacent C atom around

the N dopant, gaining approximately a $0.36e$ charge to elongate the O–O bond by 0.06 Å. The $O_2$ is then transferred from the $^3\Sigma_g^-$ triplet ground state to the $^1\Delta_g$ singlet excited state.

**3.1.2 Catalytic properties of $C_{59}B$ and its oxide.** In order to examine the catalytic properties of the singly doped fullerene, we studied the oxidization reaction of the CO molecule. As both the $O_2$ and CO could be absorbed onto $C_{59}B$, we started our studies from their co-adsorption configuration. The optimized co-adsorption configurations are shown in Fig. 1e and f. The configuration in Fig. 1e represents the adsorption process of the

$O_2$ approaching $C_{59}B$ first, and Fig. 1f shows the process with CO adsorption being followed by an $O_2$ molecule approaching. According to our calculations, the configuration in Fig. 1e is approximately 0.12 eV lower in total energy. Starting from the lowest energy co-adsorption configuration, we carefully studied the CO oxidization reaction path, which is shown in Fig. 1g. We have also calculated the frequencies of the stationary point structures during the reaction, the results are shown in Fig. S3 in the ESI.† The frequencies of the reactants and products are positive, while the transition states have only one imaginary mode. An energy of 0.48 eV could activate the reaction. As shown in the inset image showing the structure of saddle point B in Fig. 1g, the reaction would start with the dissociation of an $O_2$ molecule to provide an atomic O for CO oxidation through the Eley–Rideal (ER) mechanism, which then moves into a meta-stable state. One of the dissociated O atoms connects with the B atom and its nearest C atom to oxidize the $C_{59}B$. Another O atom connects with B and the C of the CO molecule simultaneously, forming a complex O–C–O species. Then, an activation energy of 0.44 eV could desorb the O–C–O to release an $CO_2$ molecule. Referring to the whole reaction path, we conclude that the energy barrier is about 0.48 eV and this was used to determine the reaction rate for this reaction, as shown in Fig. 1g.

The reaction product $C_{59}BO$, as shown in Fig. 2a, could be further used as a catalyst. First, we consider the case of a CO molecule approaching the O atom in the $C_{59}BO$ oxide, which was found to have an energy barrier of approximately 1.47 eV in the converged reaction path shown in Fig. 1h, this limits its occurrence. Interestingly, the B atom in $C_{59}BO$ oxide is still able to bond an $O_2$ molecule. There is only a 0.02 eV energy barrier for $O_2$ adsorption, which forms a 1.54 Å BO bond in the end-on adsorption configuration shown in Fig. 2b, the adsorption energy is −0.76 eV. The O–O bond was found to be elongated by 0.08 Å. A charge gain of approximately $0.64e$ was confirmed by our Bader charge analysis for $O_2$, which helps to transfer it from a $^3\Sigma_g^-$ triplet state to a $^1\Delta_g$ singlet state. As shown in Fig. 2g, a CO could approach the adsorbed $O_2$ to form the O–O–C–O complex species through the Langmuir–Hinshelwood (LH) oxidization mechanism by overcoming the 0.63 eV energy barrier, which would evolve to release a $CO_2$ molecule under a 0.21 eV activation energy, leaving a single O atom adsorbed on the B atom. Providing that it is used in the CO-rich surrounding conditions, the produced atomic O could be removed from the $C_{59}BO$ oxide through oxidization of one more of the CO molecules (the barrier is 0.11 eV). Otherwise, it would directly react with the doped fullerene to form $C_{59}BO_2$ oxide (see the structures shown in Fig. 2c), which require a 0.17 eV activation energy. It should be mentioned here that the $C_{59}BO_2$ oxide could also be obtained from the lowest energy chemisorption state of $O_2$ on $C_{59}B$ under a 0.24 eV activation energy for $O_2$ dissociation and then after the oxidization process. After this, one more $O_2$ could rapidly be attached onto the $C_{59}BO_2$ oxide (see Fig. 2d for adsorption configuration), which could then be used to oxidize one more CO under a 0.37 eV activation energy along the converged pathway presented in Fig. 2h to produce a $CO_2$ molecule and an atomic O. For the $O_2$ adsorption on the

$C_{59}BO_2$ oxide, a charge of approximately $0.70e$ is transferred from the oxide to the $O_2$ molecule, making the triplet-singlet state transition which elongates the O–O bond by 0.10 Å. The produced atomic O would either oxidize one more CO or directly react with $C_{59}BO_2$, depending on whether it is protected by CO molecules or not. The oxidization of CO requires an activation of 0.11 eV, while the barrier is 0.09 eV for the oxidization of $C_{59}BO_2$ to form $C_{59}BO_3$ oxide (see Fig. 2e for the geometrical configuration). Again, an $O_2$ molecule could be adsorbed onto the B atom through an exothermal adsorption process, forming a 1.23 eV lower end-on chemisorption state, which is also transferred into the $^1\Delta_g$ singlet excited state by gaining a ~$0.73e$ charge. Correspondingly, the O–O is elongated by 0.10 Å. As shown in Fig. 2i and j, the $C_{59}BO_3$ oxide could be repeatedly used as a catalyst for CO oxidization. Therefore, in the process of CO oxidization on $C_{59}B$, the doped fullerene would have the chance to change to the new catalyst species, $C_{59}BO_3$ oxide. The corresponding rate determining barrier is only 0.59 eV for the CO oxidization cycles catalyzed by $C_{59}BO_3$ oxide, showing a good catalytic performance. In addition, we have also calculated the CO adsorption on nicked $C_{59}BO_x$ ($x = 1$–3) oxides, which are only weakly adsorbed and could be easily removed from the $C_{59}BO_x$ oxides to leave the B atom for $O_2$ adsorption. The superior catalytic properties of the $C_{59}BO_x$ oxides are mainly associated with the activation of the adsorbed $O_2$. In addition, in Fig. 2k and l, we present the optimized reaction pathway starting from another CO–$O_2$ co-adsorption state as shown Fig. 1f. The CO would be oxidized by the LH oxidization mechanism releasing an $CO_2$ molecule and producing the $C_{59}BO$ oxide, for which the higher energy barrier is 0.51 eV. Again, the produced $C_{59}BO$ oxide could be further used to catalyze CO oxidizations through the reactions studied in Fig. 2g–j to finally obtain the $C_{59}BO_3$ oxide. Also, for the $C_{59}B$ oxide materials, we have carried out FPMD simulations. The $C_{59}BO$, $C_{59}BO_2$, and $C_{59}BO_3$ were found to be well preserved in our 5 ps simulations at 1000 K, suggesting their stabilities.

**3.1.3 Catalytic properties of $C_{59}N$ and its oxide.** Unlike $C_{59}B$, $C_{59}N$ could only chemically adsorb $O_2$. The adsorption process is barrierless and the stable state is a 0.29 eV lower end-on configuration. Our Bader charge analysis shows approximately a $0.37e$ charge transfer from $C_{59}N$ to $O_2$, transferring it from the $^3\Sigma_g^-$ triplet ground state to the $^1\Delta_g$ singlet excited state. The O–O bond was found to be elongated by 0.07 Å. On $C_{59}B$, the best adsorption site for $O_2$ is on top of the B dopant. However, the N dopant in $C_{59}N$ is not the active site, however, this makes the surrounding C atoms active. Our calculations show that the adsorption of $O_2$ would only develop an O–C bond with the nearest C atom. The lowest chemisorption adsorption state of $O_2$ on $C_{59}B$ with O–O being parallel to the B–C bond is not stable in the case of $O_2$ adsorption on $C_{59}N$. The adsorption of $O_2$ on $C_{59}N$ increases the O–O bond length by 0.06 Å. An incoming CO molecule could be oxidized by overcoming the 0.44 eV energy barrier (see Fig. 3d). The produced single O atom could be easily removed by one more CO providing that it is in the CO-rich surrounding conditions to provide sufficient CO molecules around the catalyst. Otherwise, this O would directly react with fullerene to form the $C_{59}NO$ oxide by overcoming
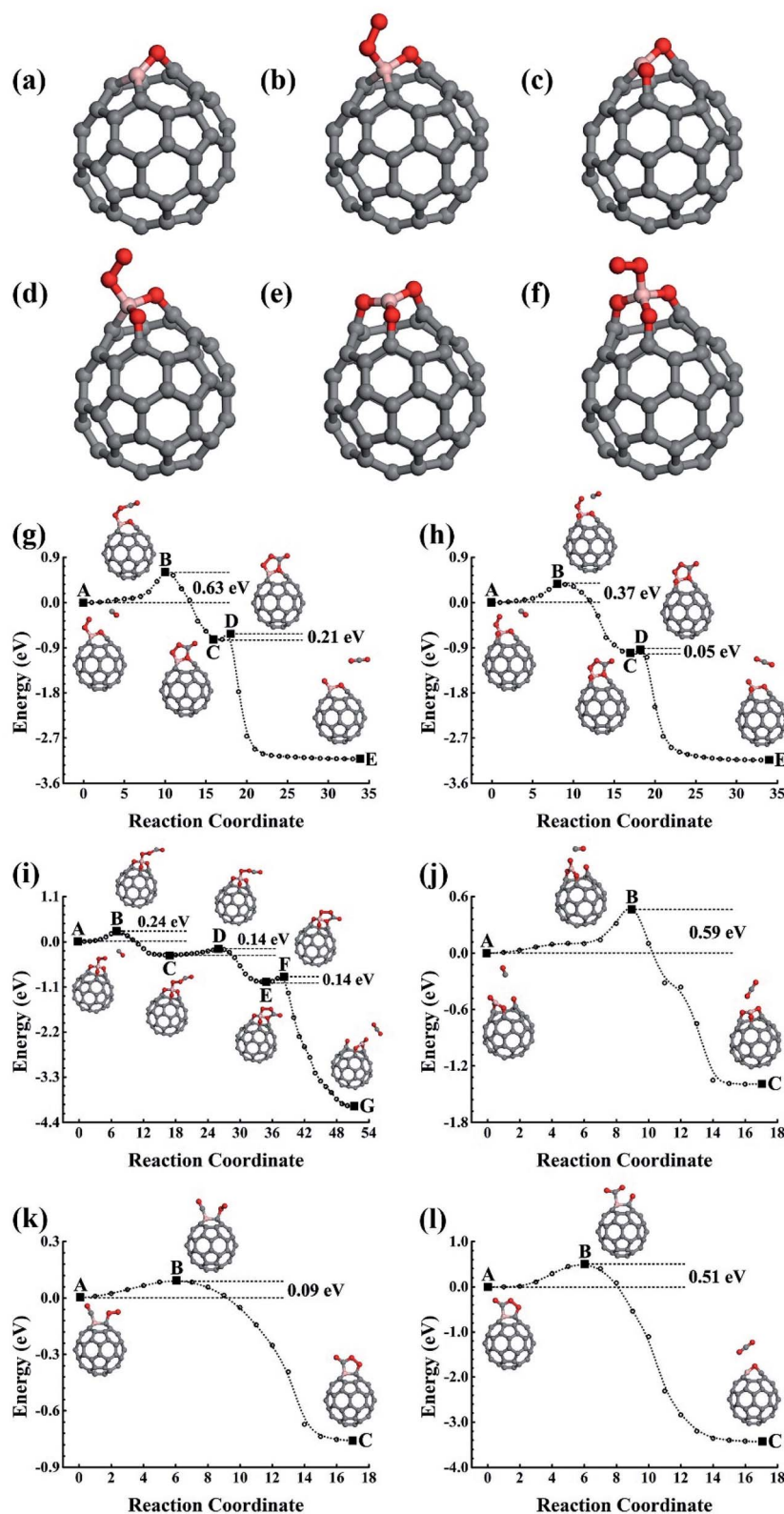
Fig. 2 (a)−(f) Show the structural skeleton illustrations for $C_{59}BO$, $C_{59}BO_2$, $C_{59}BO_3$ oxides, and the $O_2$ molecule adsorption configurations on the different oxide structures of $C_{59}B$, respectively. (g)−(l) Show the reaction paths for CO oxidization on $C_{59}B$ oxide catalysts. The initial, final, saddle, and meta-stable intermediate states are illustrated by the inset images. C, B, and O are represented by the grey, pink, and red balls.

a 0.20 eV energy barrier, which is found to have a good stability using our FPMD simulations performed for 5 ps at 1000 K. The geometrical structures of the $C_{59}NO$ oxide and the corresponding chemisorption state of a $O_2$ molecule upon it are shown in Fig. 3a and b, respectively. The adsorption of $O_2$ onto the $C_{59}NO$ oxide gains approximately a 0.45$e$ charge to elongate
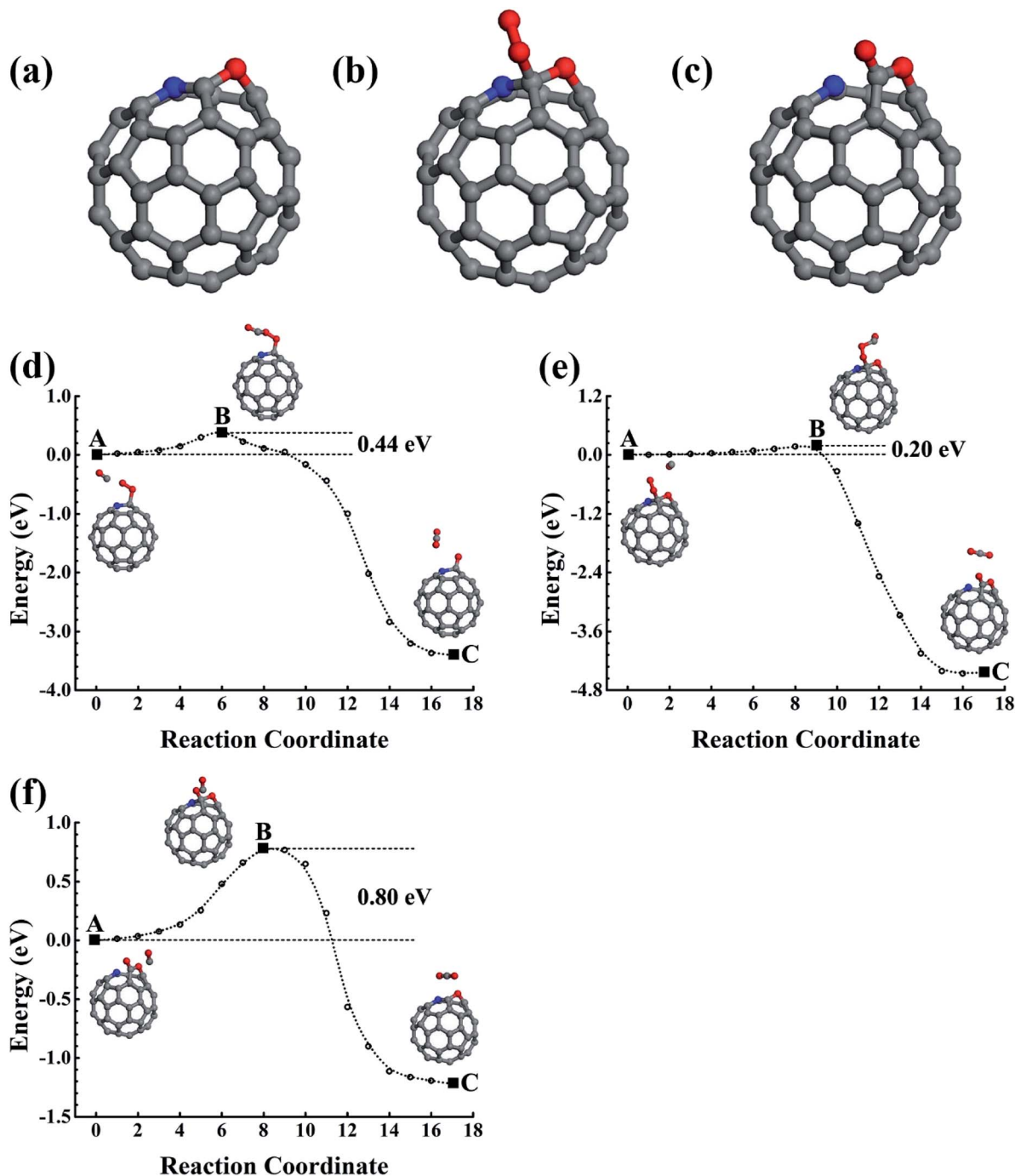
**Fig. 3** (a) Structural skeleton illustrations for the $C_{59}NO$ oxide; and (b) the lowest energy structure of $O_2$ molecules on the $C_{59}N$ oxide. (c) The structure of $C_{59}NO_2$. (d)–(f) The optimized reaction paths for CO oxidization on $C_{59}N$ and its oxides catalysts. The initial, final, saddle, and meta-stable intermediate states are illustrated in the inset images. C, N, and O are represented by the grey, blue, and red balls.

the O–O bond by 0.10 Å to reach the $^1\Delta_g$ singlet excited state. In Fig. 3e and f, we studied the catalytic performance of the $C_{59}NO$ oxide for CO oxidation. The rate determining barrier was found to be 0.80 eV. In contrast to that observed for the B doped fullerene, the $C_{59}NO$ oxide species would repeatedly act as a oxide catalyst in the successive CO oxidation cycles. The atomic O produced in the reaction shown in Fig. 3e does not like to move to the bridge sites to form two bonds with fullerene

simultaneously (see Fig. 3c), and would therefore remain to catalyze another CO molecule through the reaction shown in Fig. 3f to produce $CO_2$ and $C_{59}NO$ oxide.

**3.1.4 Discussion on the catalytic properties of $C_{60-n}X_n$ (X = B or N, and $n$ = 1, 2).** As discussed above, both $C_{59}B$ and $C_{59}N$ can catalyze CO oxidations. The CO oxidization or the $O_2$ dissociation occurs in the initial catalytic reaction on $C_{59}B$ and helps to produce a stable $C_{59}BO_3$ oxide catalyst, which could be

further used repeatedly as a catalyst species. The CO oxidization on $C_{59}BO_3$ oxide is found to have a rate determining energy barrier of 0.59 eV, showing a good catalytic performance. By using $C_{59}N$ in the CO-rich conditions to provide sufficient CO to protect $C_{59}N$ against oxidation, it could be kept as a repeating catalyst species. The corresponding rate determining barrier is 0.44 eV, which also shows the good catalytic ability of N doped fullerene. If there is not enough CO gas to surround the $C_{59}N$, it may also be oxidized during the reaction to form $C_{59}NO$ oxide. Compared to the $C_{59}N$, the catalytic ability of $C_{59}NO$ is reduced, and would require 0.80 eV as a rate determining activation energy to oxidize CO in the successive oxidization cycles. Also, in order to facilitate further theoretical and experimental studies, we calculated the vibration properties of the initial and final states of the above described reaction paths and no imaginary frequency was found. An imaginary vibrational mode is found for the corresponding transition state. The calculated frequencies are provided in Fig. S3 in the ESI.†

In addition to the singly doped fullerene, a low doping concentration structure will probably also be generated during the fabrication of doped fullerene. Previous studies have shown that the B(N) dopants prefer to separately substitute the carbon atom in fullerene.[28–30] For example, the best doping configurations for the two B and N atoms are that the dopants substitutionally occupy the opposite sites of a $C_6$ hexagon. In our studies, we have studied the catalytic properties of the best doping configurations of $C_{58}B_2$ and $C_{58}N_2$. Like the singly doped fullerene, they evolve into the oxide materials after the first few catalytic cycles for catalyzing CO oxidizations. When compared to the oxides of $C_{59}B$ and $C_{59}N$, our calculations do not show obvious synergetic effects on the catalytic properties of the $C_{58}B_2$ and $C_{58}N_2$ oxides (see Fig. S1 and S2 in the ESI†).

## 3.2 BN-pair doped fullerene

In the experiment, the B and N can also co-doped in fullerene, and the B–N bond is probably formed in the lowest energy doping configuration. The B–N bonding obviously affects their effects upon the co-doped nanostructures, which could be used to engineer the physical and chemical properties of the carbon nanostructures. With the purpose of helping design high-performance nanostructures in the experiments, we also carried out careful studies on the BN-pair doped fullerene to shed light on the catalytic properties of the low-concentration substitution doping configurations of the B–N co-doped carbon nanostructures. The stability of the BN-pair doped fullerene has also been confirmed using FPMD simulations performed for 5 ps at 1000 K.

### 3.2.1 Catalytic properties of $C_{58}BN$. The lowest energy doping configuration occurs when the BN pair substitutionally replaces a C–C pair. On $C_{58}BN$, both the $O_2$ and CO allow chemical adsorption. Fig. 4a and b shows the $O_2$ adsorptions in the configurations with an O–O bond as being parallel to the fullerene, which have close adsorption energies (about −0.29 eV). In addition, we have also optimized the geometrical structure by placing O–O parallel above the B–N bond. During the optimization, the $O_2$ would however be pushed away, which

is reasonable considering the inert nature of the B–N bond. However, the doping destroys the ideal π-electron conjugate integrity on pure fullerene. By considering the substitutional arrangement of dopant atoms in $C_{60}$ as the doping structural fragment (DSF) of the $C_{58}BN$ configuration, the other part which only consists of a C atom can be discussed as the undoped structural fragment (USF). The density of the π-electron distribution above the DSF would be reduced in comparison to the distribution above the USF, making the adjacent space between them active for gas molecule adsorption. Like the adsorption of CO onto the B doped fullerene, CO prefers the end-on adsorption configuration (see Fig. 4c), developing a C–B bond and releasing 0.34 eV of energy. In Fig. 4d, the co-adsorption of CO and $O_2$ is illustrated. The shortest atomic distance between CO and $O_2$ is 3.7 Å, hinting at the weak interaction between them. Our NEB method studies show a 1.22 eV energy barrier for the oxidization reaction to occur between them, which would reduce the possibility of this reaction occurring. Our results show that the B–N co-doped $C_{60}$ has similar catalytic properties to the B–N co-doped graphene. In both cases, B serves as the active center.[50]

### 3.2.2 Catalytic properties of the $C_{58}BN$ oxide. As with the B and N doped fullerene, the BN-pair doped fullerene can also be oxidized to form $C_{58}BNO_2$. This can be obtained by the dissociation of the pre-adsorbed $O_2$ to produce atomic O atoms to oxidize the $C_{58}BN$, for which the energy barrier is only around 0.12 eV. Also, providing the catalyst is to be used in CO-rich surrounding conditions, the first few CO oxidization cycles would also help generate the $C_{58}BNO_2$ oxide. As illustrated in Fig. 4e, our first-principles structural optimizations confirm that the configuration shown in the Fig. 4e is the lowest energy oxidization structure, in which the O oxidation occurs around the B atom. It is 2.19 eV lower in energy than the configuration in which the O oxidization occurred around the N atom. In addition, the oxidization around the B atom in the lowest energy configuration shown in Fig. 4e would in turn hinder the $O_2$ adsorption around the N atom. Therefore, we propose that the Fig. 4e configuration accounts for the main oxide species and would dominate the catalytic performance accordingly. The $O_2$ can be adsorbed onto the $C_{58}BNO_2$ oxide without an energy barrier, which has an absorption energy of −0.56 eV. Approximately a 0.65$e$ charge transfer is found to occur between the $C_{58}BNO_2$ oxide and the adsorbed $O_2$ molecule, which excites it into the $^1\Delta_g$ singlet state and elongates the O–O bond by 0.09 Å. In Fig. 4f and g, we have evaluated the catalytic properties. Surprisingly, the rate determining barrier is found to be only 0.42 eV along the entire catalytic cycle. In addition, our FPMD simulations also suggest the stability of $C_{58}BNO_2$ at 1000 K. As for the product of a single O atom adsorbed onto the $C_{58}BNO_2$ oxide (see the inset image in Fig. 4g), our structural optimization shows that the single atomic O would not move to the adjacent bridge site upon formation of a B–N bond. The inert BN bond helps keep it at on the top site to retain good reactivity to oxidize the CO molecule. Compared to the barriers of CO oxidation catalyzed by B or N doped fullerene, the BN-pair doping shows synergetic effects to enhance the catalytic properties correspondingly. Also, our calculations of the frequencies
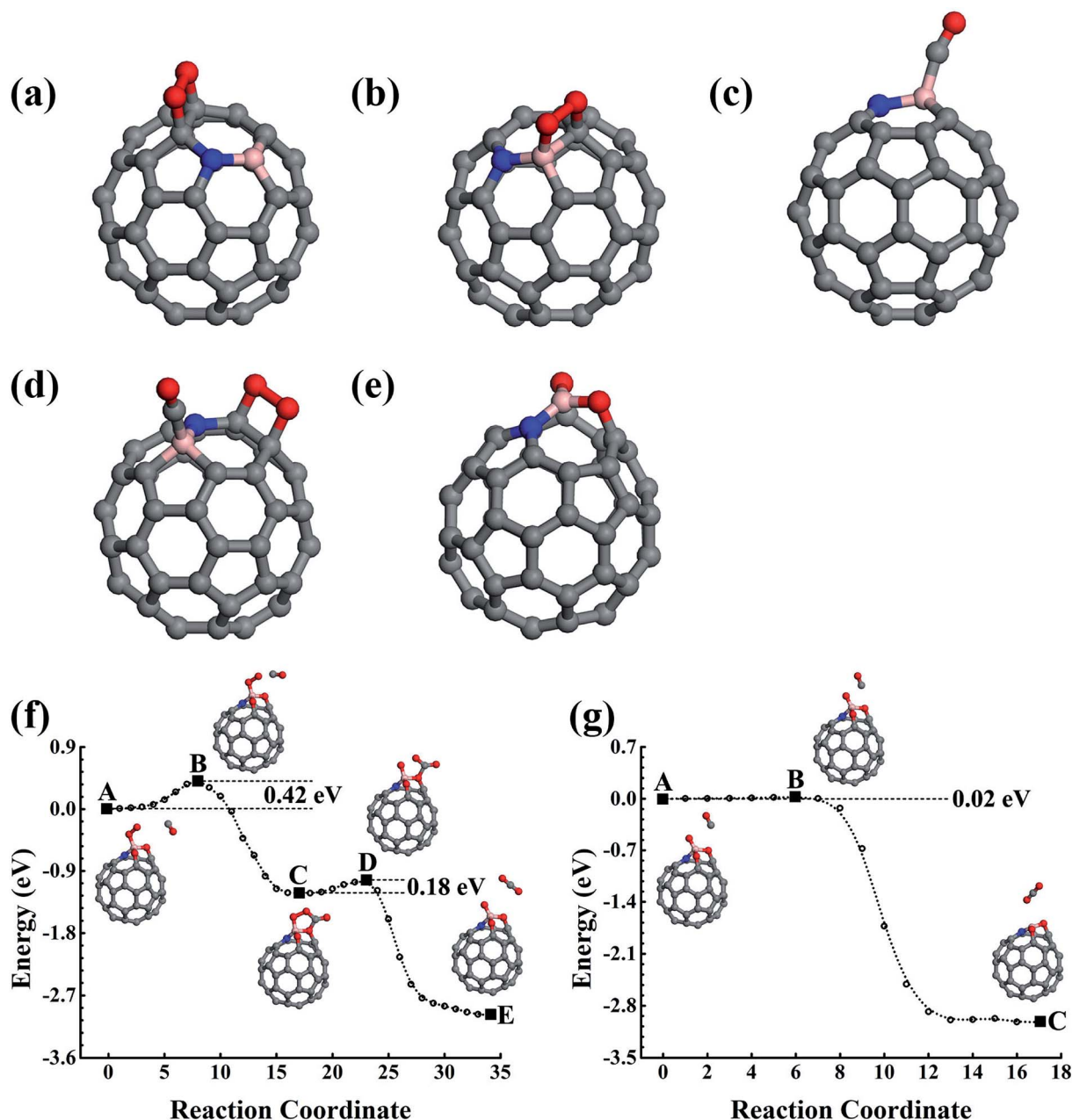
Fig. 4   The structures of O$_2$ adsorption (a) and (b), CO adsorption (c), and CO and O$_2$ co-adsorption (d) on C$_{58}$BN. (e) The structure of C$_{58}$BNO$_2$ oxide. (f) and (g) The reaction pathways for CO oxidization catalyzed by C$_{58}$BNO$_2$ oxide. C, B, N, and O are represented by the grey, pink, blue, and red balls.

of the reactants and products only show positive frequencies, suggesting their stability in the experimental fabrications. Again, the calculation only shows one negative frequency for the corresponding transition state, confirming the validity of the elastic band method for searching for the saddle point (see Fig. S3, ESI†).

### 3.3   B$_3$N and BN$_3$ doped fullerene

In addition to the smallest stoichiometric BN-pair doping, we also estimated the nonstoichiometric B–N doping in fullerene. The B$_3$N(BN$_3$), with the N(B) being surrounded by three B(N)

atoms, were used as examples to illustrate the B- and N-rich nonstoichiometric co-doping. The doping configurations are shown in Fig. 5a and b, which are confirmed by our structural optimizations as being the lowest energy doping configurations. We also performed 5 ps FPMD simulations at 1000 K for the lowest energy doping configurations of C$_{56}$B$_3$N and C$_{56}$BN$_3$, which suggested that they were stable.

**3.3.1   Catalytic properties of C$_{56}$B$_3$N.** In the C$_{56}$B$_3$N nanostructure, owing to the fact that the B atoms are separately distributed around the center N atom, the co-adsorption of O$_2$ and CO on different B atoms is also well separated, which could
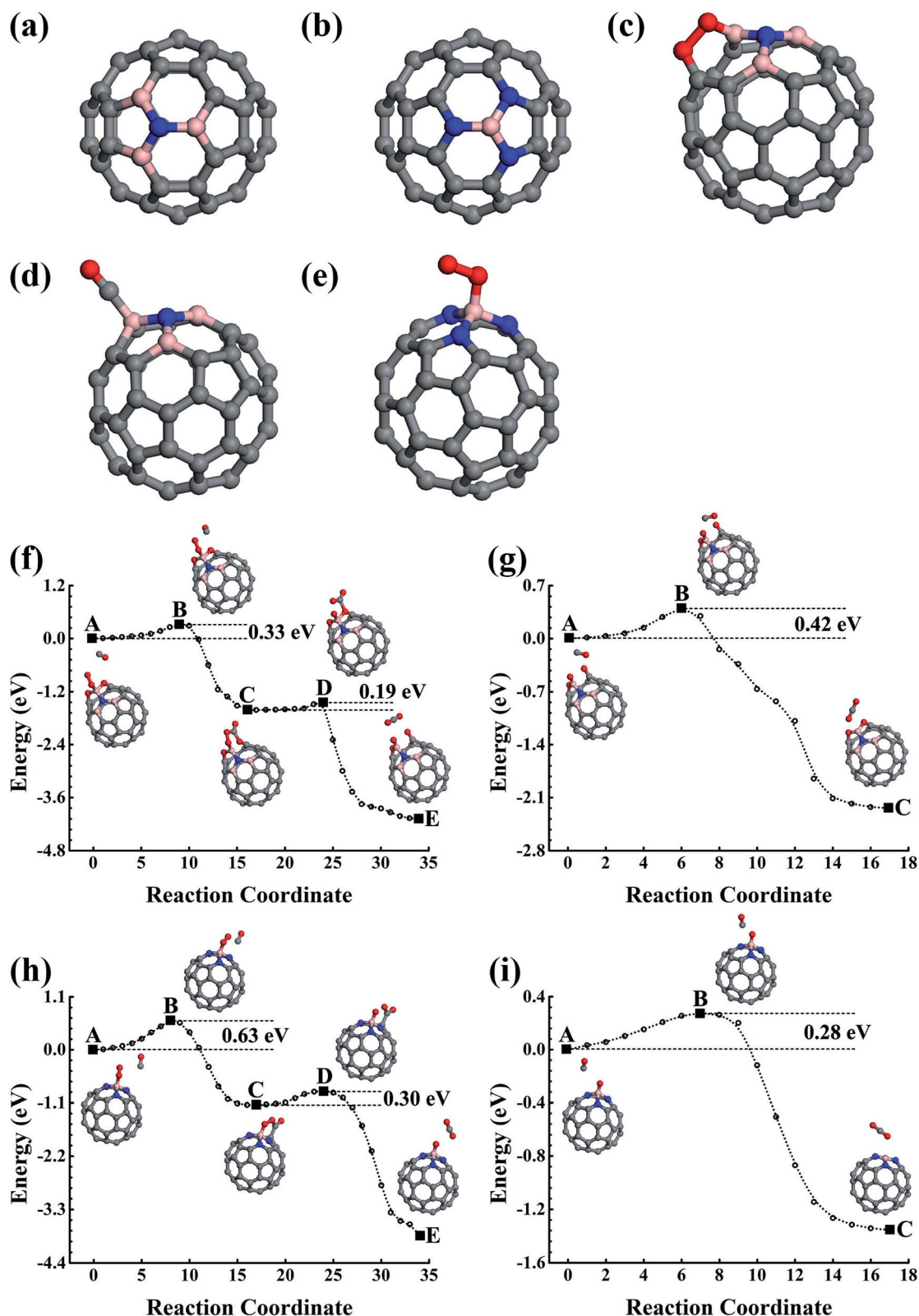
Fig. 5 (a)–(e) Structures of B$_3$N and BN$_3$ doped fullerenes and the corresponding gas molecule adsorption configurations on them. (f) and (g) The reaction pathways of CO oxidizations catalyzed by the C$_{56}$B$_3$N oxide. (h) and (i) Reactions catalyzed by C$_{56}$BN$_3$. C, B, N, and O are represented by the grey, pink, blue, and red balls.

hinder a direct reaction between them. Therefore, in our studies, we concentrated on examining the catalytic properties of the B atom and its nearest N or C atoms. Both O$_2$ and CO were found to prefer being adsorbed on the B atom with −1.55 and −0.65 eV adsorption energies, respectively. The corresponding adsorption configurations are provided in Fig. 5c and d. The

adsorbed $O_2$ gains an approximately $1.33e$ charge from $C_{56}B_3N$, which elongates the O–O bond by 0.27 Å to transfer it from the triplet ground state to the singlet excited state. Starting from the small molecule adsorption states, we calculated three reactions, the dissociation of $O_2$ to directly oxidize $C_{56}B_3N$, the oxidation of the incoming COs by the pre-adsorbed $O_2$ to finally generate the $C_{56}B_3N$ oxide, and the oxidation of the pre-adsorbed CO by the incoming $O_2$ to finally obtain the $C_{56}B_3N$ oxide. Judging by the largest energy barrier of 0.48 eV found in these reactions, the final oxide $C_{56}B_3NO_2$ could be obtained. We have estimated the stability of $C_{56}B_3NO_2$ using FPMD simulations, which was found to be well preserved during the 5 ps simulations at 1000 K. Then, using $C_{56}B_3NO_2$ oxide as a prototype, we optimized the minimum energy reaction paths for successive CO oxidations which are shown in Fig. 5f and g. An $O_2$ molecule could be adsorbed onto $B_{56}B_3NO_2$ to be activated to help oxidize an incoming CO and finally release an $CO_2$ molecule. Our Bader charge analysis shows approximately a $0.70e$ charge gain of $O_2$, which helps elongate the O–O bond by 0.10 Å. The largest energy barrier for the reactions shown in Fig. 5f is 0.33 eV. After this, one more CO molecule can react with the produced O atom to release another $CO_2$ and restore the geometrical structure of $B_{56}B_3NO_2$, allowing it to be used as recycled catalyst species in successive catalytic reaction cycles. The corresponding rate determining energy barrier is only 0.42 eV.

**3.3.2 Catalytic properties of $C_{56}BN_3$.** In the $C_{56}BN_3$ nanostructure, the B atom surrounded by three N atoms was also found to be an active site for gas molecule adsorption. Our calculations show that only $O_2$ could be adsorbed, which can connect with the central B atom in the end-on adsorption state as shown in Fig. 5e. The adsorption energy is −1.41 eV and the O–O is elongated by 0.12 Å, activating the $O_2$ into its $^1\Delta_g$ singlet state to help oxidize CO. Also, a charge gain of approximately $0.80e$ was found in our Bader analysis. During the process of CO approaching the $O_2$, it encounters an energy barrier of 0.63 eV to react with the $O_2$ to form an O–O–C–O complex species attached onto $C_{56}BN_3$ with an O–B and a C–C bond. Under the 0.3 eV activation energy, this metastale state could further release an $CO_2$ molecule and leave an atomic O capped onto the central B. In contrast to the case of the single B doped fullerene, the surrounding B–N bonds help hinder the oxidation of $C_{56}BN_3$ to retain the atomic O atom, which can then be easily removed by catalyzing the successive CO oxidation. The energy barrier is 0.28 eV. Once the produced $CO_2$ molecule is released, the $C_{56}BN_3$ can be restored, which can be used again in the successive CO oxidization cycles, showing good recycling properties.

**3.3.3 Discussion on the catalytic properties of $B_3N$ and $BN_3$ doped fullerenes.** Based on the above described results, one can see that the active sites are located around the B atom in both the $B_3N$ and $BN_3$ doped fullerenes, consisting of the BN-pair doped fullerene. The $B_3N$ doped fullerene can be oxidized after a few cycles for catalyzing CO oxidations. The oxidized nanostructure is found to have good catalytic properties and good recycling properties. In contrast, the N atoms surrounding the central B in the $BN_3$ doped fullerene can help maintain the geometric structure of $C_{56}BN_3$ for

catalyzing the CO oxidization. The $BN_3$ doped structure can be repeatedly used for catalyzing the CO oxidization with a rate determining energy barrier of 0.63 eV. In addition, we have studied the vibrational properties of the initial and final states of the CO oxidations catalyzed by the $B_3N$ or $BN_3$ doped fullerenes, which supports their stabilities (no negative frequencies). The corresponding transition state was found to have only one imaginary frequency, suggesting that it is the saddle point state (see Fig. S3, ESI†). Again, we used DSF to account for the doping structural fragment of the geometrical distribution of dopant atoms. Our studies show that the B dopant at either the edge of the DSF fragment or the site close to the edge may have good catalytic properties, and it would be worthwhile performing detailed experimental and theoretical studies in order to design high-performance and durable nanocatalysts.

# 4. Conclusions

Using elastic band method calculations based on first-principles studies, we have carefully studied low-concentration B and N doped and their co-doped fullerenes. Both $C_{59}B$ and $C_{59}N$ show good catalytic properties for catalyzing CO oxidation, which could also be capable of being oxidized during the first few catalytic reaction cycles. The corresponding oxides were found to have superior catalytic properties, which could be repeatedly used as a catalyst showing durable properties as well. The CO and $O_2$ could be co-adsorbed onto $C_{59}B$. The co-adsorption configurations require 0.48 or 0.44 eV activation energies to make the CO oxidation occur and produce a $C_{59}BO$ oxide simultaneously, which could be further oxidized in the successive CO oxidation processes to obtain a $C_{59}BO_3$ oxide. In addition, the single $O_2$ adsorption on $C_{59}B$ can also oxidize it with a 0.24 eV barrier. Providing it is used in CO-rich conditions, $C_{59}N$ could retain its structure as a recycling catalyst for CO oxidation. A 0.44 eV rate determining barrier is found. Otherwise, after oxidizing the CO, the produced atomic O atom can overcome the 0.20 eV to oxidize the $C_{59}N$. Both the $C_{59}B$ and $C_{59}N$ oxides could be used as durable recycling catalysts, which are found to have 0.59 and 0.80 eV rate determining energy barriers, respectively. Interestingly, the co-doping of B and N in low concentration doping fullerene may have superior catalytic properties. The BN-pair doped fullerene would also be oxidized. The produced $C_{58}BN$ oxide can help to oxidize CO with a 0.42 eV rate determining barrier. For the nonstoichiometric $B_3N$ and $BN_3$ species, their doping in fullerene is also found to have superior catalytic properties. The B atoms either at the doping domain edge in $B_3N$ or at the doping center in $BN_3$ are active sites. $C_{56}B_3N$ can be oxidized during catalyzing CO oxidations. The resulting $C_{56}B_3N$ oxide has a rate determining barrier of 0.42 eV for catalyzing successive CO oxidations. In $C_{56}BN_3$, the central B is protected by its surrounding N atoms against oxidization to remain as a recycling catalytic active site for CO oxidation, which is found to have a 0.63 eV rate determining energy barrier.

## Conflicts of interest

There are no conflicts of interest to declare.

## Acknowledgements

## References

1 H. Falsig, B. Hvolbœk, I. S. Kristensen, T. Jiang, T. Bligaard, C. H. Christensen and J. K. Nørskov, *Angew. Chem., Int. Ed.*, 2008, **47**, 4835.

2 Z.-P. Liu and P. Hu, *J. Am. Chem. Soc.*, 2002, **124**, 14770.

3 H.-T. Chen, J.-G. Chang, S.-P. Ju and H.-L. Chen, *J. Comput. Chem.*, 2010, **31**, 258.

4 J. L. C. Fajín, M. N. D. S. Cordeiro and J. R. B. Gomes, *J. Phys. Chem. C*, 2008, **112**, 17291.

5 J. Xu, T. White, P. Li, C. He, J. Yu, W. Yuan and Y.-F. Han, *J. Am. Chem. Soc.*, 2010, **132**, 10398.

6 H.-L. Chen, C.-H. Su and H.-T. Chen, *Chem. Phys. Lett.*, 2012, **536**, 100.

7 J. Zhang, H. Jin, M. B. Sullivan, F. C. H. Lim and P. Wu, *Phys. Chem. Chem. Phys.*, 2009, **11**, 1441.

8 H.-Y. Su, M.-M. Yang, X.-H. Bao and W.-X. Li, *J. Phys. Chem. C*, 2008, **112**, 17303.

9 X.-Q. Gong, Z.-P. Liu, R. Raval and P. Hu, *J. Am. Chem. Soc.*, 2004, **126**, 8.

10 J. T. Hirvi, T.-J. J. Kinnunen, M. Suvanto, T. A. Pakkanen and J. K. Nørskov, *J. Chem. Phys.*, 2010, **133**, 084704.

11 S.-H. Oh and G. B. Hoflund, *J. Catal.*, 2007, **245**, 35.

12 H.-T. Chen, *J. Phys. Chem. C*, 2012, **116**, 6239.

13 H.-T. Chen and J.-G. Chang, *J. Phys. Chem. C*, 2011, **115**, 14745.

14 L.-C. Hsu, M.-K. Tsai, Y.-H. Lu and H.-T. Chen, *J. Phys. Chem. C*, 2012, **117**, 433.

15 M. Huang and S. Fabris, *J. Phys. Chem. C*, 2008, **112**, 8643.

16 Z.-P. Liu, X.-Q. Gong, J. Kohanoff, C. Sanchez and P. Hu, *Phys. Rev. Lett.*, 2003, **91**, 266102.

17 C.-M. Wang, K.-N. Fan and Z.-P. Liu, *J. Am. Chem. Soc.*, 2007, **129**, 2642.

18 G. Chen, S. J. Li, Y. Su, V. Wang, H. Mizuseki and Y. Kawazoe, *J. Phys. Chem. C*, 2011, **115**, 20168.

19 X. Fan, J. Li and G. Chen, *RSC Adv.*, 2017, **7**, 17417.

20 D. W. Yuan, Z. R. Liu and J. H. Chen, *J. Chem. Phys.*, 2011, **134**, 054704.

21 D. W. Yuan and Z. Zeng, *J. Chem. Phys.*, 2004, **120**, 6574.

22 J. Zhang, Z. Fu, Z. Yang and S. F. Li, *Phys. Lett. A*, 2012, **376**, 3235.

23 Y.-P. Xie and X.-G. Gong, *J. Chem. Phys.*, 2010, **132**, 244302.

24 X. Chen, *Phys. Chem. Chem. Phys.*, 2015, **17**, 29340.

25 J. Duan, S. Chen, M. Jaroniec and S. Z. Qiao, *ACS Catal.*, 2015, **5**, 5207.

26 X. Fan, G. Zhang and F. Zhang, *Chem. Soc. Rev.*, 2015, **44**, 3023.

27 Y. Zheng, Y. Jiao, M. Jaroniec and S. Z. Qiao, *Angew. Chem., Int. Ed.*, 2013, **52**, 3110.

28 M. R. Manaa, *Solid State Commun.*, 2004, **129**, 379.

29 M. R. Manaa, D. W. Sprehn and H. A. Ichord, *J. Am. Chem. Soc.*, 2002, **124**, 13990.

30 M. R. Manaa, H. A. Ichord and D. W. Sprehn, *Chem. Phys. Lett.*, 2003, **378**, 449.

31 X. B. Hu, Y. T. Wu and Z. B. Zhang, *J. Mater. Chem.*, 2012, **22**, 15198.

32 I. H. Lin, Y. H. Lu and H.-T. Chen, *Phys. Chem. Chem. Phys.*, 2016, **18**, 12093.

33 I.-H. Lin, Y.-H. Lu and H.-T. Chen, *J. Comput. Chem.*, 2017, **38**, 2041.

34 R. Krishnan, S.-Y. Wu and H.-T. Chen, *Carbon*, 2018, **132**, 257.

35 M. D. Esrafili, R. Mohammad-Valipour, S. M. Mousavi-Khoshdel and P. Nematollahi, *ChemPhysChem*, 2015, **16**, 3719.

36 Y. Tang, W. Chen, Z. Shen, S. Chang, M. Zhao and X. Dai, *Carbon*, 2017, **111**, 448.

37 Y. Tang, Z. Liu, X. Dai, Z. Yang, W. Chen, D. Ma and Z. Lu, *Appl. Surf. Sci.*, 2014, **308**, 402.

38 S. Sinthika, E. M. Kumar and R. Thapa, *J. Mater. Chem. A*, 2014, **2**, 12812.

39 S. Nigam and M. Chiranjib, *ACS Nano*, 2008, **2**, 1422.

40 G. Kress and J. Furthmüller, *Phys. Rev. B: Condens. Matter Mater. Phys.*, 1996, **54**, 11169.

41 G. Kress and D. Joubert, *Phys. Rev. B: Condens. Matter Mater. Phys.*, 1999, **59**, 1758.

42 J. P. Perdew, K. Burke and M. Ernzerhof, *Phys. Rev. Lett.*, 1996, **77**, 3865.

43 G. Mills, H. Jónsson and G. K. Schenter, *Surf. Sci.*, 1995, **324**, 305.

44 G. Henkelman and H. Jónsson, *J. Chem. Phys.*, 2000, **113**, 9978.

45 G. Henkelman and H. Jónsson, *J. Chem. Phys.*, 1999, **111**, 7010.

46 W. Tang, E. Sanville and G. Henkelman, *J. Phys.: Condens. Matter*, 2009, **21**, 084204.

47 Q. Z. Li, J. J. Zheng, J. S. Dang and X. Zhao, *ChemPhysChem*, 2015, **16**, 390.

48 Y. Wang, M. Jiao, W. Song and Z. Wu, *Carbon*, 2017, **114**, 393.

49 F. Gao, G. Zhao, S. Yang and J. Spivey, *J. Am. Chem. Soc.*, 2013, **135**, 3315.

50 C. Ricca, F. Labat, C. Zavala, N. Russo, C. Adamo, G. Merino and E. Sicilia, *J. Comput. Chem.*, 2018, **39**, 637.